Size-dependent electrical and thermal properties of onion-like carbons / polyurethane composites

Ieva Kranauskaite, Jan Macutkevic, Juras Banys, Vladimir Kuznetsov, Maxime Letellier, Vanessa Fierro, Alain Celzard, Olga Shenderova

Size-dependent electrical and thermal properties of onion-like carbons / polyurethane composites

I. Kranauskaite[1], J. Macutkevic[1], J. Banys[1], V. Kuznetsov[2],
M. Letellier[3], V. Fierro[3], A. Celzard[3], O. Shenderova[4]

[1]Vilnius university, Sauletekio Ave. 9, Vilnius, Lithuania,

[2]Boreskov Institute of Catalysis SB RAS, Lavrentiev Ave. 5, Novosibirsk, Russia

[3]IJL-UMR Université de Lorraine – CNRS 7198, ENSTIB, 27 rue Philippe Seguin, BP 21042, 88051 Epinal Cedex 9, France

[4]International Technology Center, Raleigh, NC 27715, USA

Results of dielectric/electrical studies of onion-like carbon (OLC)/polyurethane composite films in very broad frequency (20 Hz – 3 THz) and temperature (26 – 300 K) ranges are presented. We show that the percolation threshold in these composites strictly depends on OLC aggregate size and is lower for composites having smaller OLC aggregates. The electrical conductivity in the composites is mainly due to electron tunnelling between OLC clusters and quasi-one-dimensional hopping inside the clusters. The thermal diffusivity increases with OLC concentration and, as for electrical conductivity, is the highest for composites having the smallest OLC aggregates.

Introduction

Polymer-based composites presenting electrical percolation have attracted much attention because of their potential applications such as electroactive or sensitive materials, or as electromagnetic coatings [1]. Thermally conductive composites also find a lot of applications, since they can be used for example as heat sink in various electric and electronic systems [2]. In binary mixtures made of electrically conducting and non-conducting phases, an electrical percolation occurs at some critical filler concentration, called percolation threshold [3]. It is an important task to reach as-low-as possible percolation threshold in order to maintain the mechanical properties of polymers and to save the cost of (generally expensive) fillers. The lowest percolation thresholds were generally observed in composites based on carbon nanotubes, due to their high aspect ratio [4]. Nevertheless, the percolation threshold in other composites, filled for instance by carbon blacks forming long chain-like aggregates, can be also very low [5]. But the percolation threshold of composites based on the same polymer matrix and on the same carbon nanotubes may take very different values [2]. This suggests that the percolation threshold is strongly influenced by the composite preparation technology. Additionally, a drawback of carbon nanotubes is their higher cost in comparison to other carbon allotropes, such as carbon blacks or graphites. Another serious disadvantage is the possible toxicity of CNTs, which has been debated for long [6], and which is still controversial today.

Herein, composites based on onion-like carbons (OLCs) are presented, which might be used for applications requesting high electrical conductivity, for example as antistatic materials, for electrostatic discharge, dissipation, electromagnetic interference shielding, temperature, pressure and gas sensors. OLCs are indeed stable, multi-shelled imperfect fullerenes, exhibiting electrical conductivity as high as about several hundred S/m at room temperature [7]. In comparison to other carbonaceous fillers, OLCs also combine many advantages such as easy preparation technology and

low cost, tuneable electrical conductivity (by annealing of OLC powder), hierarchical structure and defects which strongly absorb electromagnetic waves (required for electromagnetic shielding), and lower toxicity in comparison to carbon nanotubes [8, 9]. Many dielectric investigations of OLC-based composites were performed below the percolation threshold, where the complex dielectric permittivity of composites increases slowly with OLC concentration according to the Maxwell-Garnett theory [10, 11]. It was also demonstrated that the electronic polarizability is almost independent of the OLC morphology, but is proportional to their volume fraction [12]. Considering the electrical percolation, the threshold in OLC-polyurethane composites is 10 vol. % for OLC with mean aggregate size of 130 nm [13, 14]. Thus, the percolation threshold in OLC composites is significantly lower than the one predicted by Monte-Carlo calculations in three dimensions: 31.2 vol. % [15, 16]. The aggregate structure of conductive particles thus has a strong impact on the threshold and on the related composite dielectric/electrical properties [13], as already observed for some carbon black composites [17]. Onion-like carbons, similarly to carbon blacks, may indeed have a complex aggregate structure [7] and it was found that, in OLC-polydimethylsiloxane composites, the percolation threshold is the lowest with the smallest OLC aggregates [18].

In this work, the way of further reducing the percolation threshold in onion-like carbon / polymer composites was investigated. Therefore, the aim of this paper is to investigate the impact of OLC aggregate size on broadband electromagnetic and thermal properties of polyurethane films filled with OLC. We found that the lowest percolation threshold and the highest thermal diffusivity were obtained in OLC/PU composites having the smallest OLC aggregates (40 nm).

Experimental

The OLC samples used to prepare OLC/PU composite films were synthesized as follows. Detonation nanodiamonds (DNDs) were first obtained by detonation of a mixture of trinitrotoluene and 1,3,5 – trinitroperhydro – 1,3,5 – triazine in CO_2 atmosphere. It is known that DNDs exist in the form of strong aggregates (up to a few hundred nanometres) with coherent and incoherent interfaces between primary DND particles of size 4-7 nm [7]. The polydisperse DND material was thus separated by centrifugation into fractions with average aggregate sizes of 40 and 100 nm. Those sizes were measured by a dynamic light-scattering technique in water suspensions. The sp^2 carbon of the DND fractions was then oxidised in a mixture of concentrated sulphuric acid and chromic anhydride at 383K, and the resultant material was washed with water and dried. The powder was heated in vacuum (10^{-4} Torr) at 1923 K for 3 h. The sizes of OLC were measured by a dynamic light-scattering technique using N-Methyl-2-pyrrolidone (NMP) suspensions, in which OLC are well-dispersed. The distribution of sizes (average sizes 40 and 100 nm, respectively) was similar to that of the starting NDs in water suspensions.

Samples of OLC were subsequently mixed at different mass ratios with a Minwax “clear satin” commercial formulation of oil-based polyurethane containing 60% of volatile compounds. After mixing with the OLC powder, the polymer suspension was stirred at 400 rpm overnight at 313K. Then, the suspension was casted on a Teflon substrate and dried overnight at 318K and room pressure. The samples were thus recovered in the form of films whose typical thicknesses ranged from 0.1 to 0.8 mm, depending on the OLC concentration that modified the viscosity of the corresponding suspensions.

Scanning electron microscopy (SEM) and transmission electron microscopy (TEM) images were obtained with JSM 6460 LV and JEM 2010 electron microscopes, respectively.

The complex effective permittivity was measured as a function of frequency and temperature using a HP4284A precision LCR meter in the frequency range 20 Hz – 1 MHz. For the low-

temperature measurements, a helium closed-cycle cryostat was used, while for the high-temperature measurements a home-made furnace was used. Each measurement was started at room temperature. In the frequency range 1 MHz – 3 GHz, dielectric measurements were performed using an Agilent 8714ET vector network analyser. In the microwave frequency range from 8 to 53 GHz, a home-made waveguide spectrometer was used, applying the thin rod method, the typical value of road diameter was about several hundred micrometers [19]. In the frequency range from 1 MHz to 53 GHz, the measurement accuracy was ~ 10%. Silver paste was used for making the contacts. In the terahertz frequency range (from 100 GHz to 3 THz), an Ekspla Ltd terahertz time-domain spectrometer based on a femtosecond laser was used. The spectrometer is based on femtosecond laser fibre (wavelength 1 μm, pulse duration less than 150 fs) and GaBiAs photoconductive terahertz emitter and detector [20]. The signal to noise ratio was as high as 60 dB at the frequency 0.5 THz. The complex effective permittivity was calculated according to the Fresnel equation [21]. The measurements accuracy was better than 1% at 0.5 THz (where the signal to noise ratio is the highest) [22]. The real part σ' of the complex electrical conductivity was calculated as $\sigma' = \omega \varepsilon_0 \varepsilon''$, where ω is the angular frequency, ε_0 is the permittivity of vacuum, and ε'' is the imaginary part of the complex effective permittivity.

The thermal diffusivity was measured at room temperature with a Netzsch LFA 457 MicroFlash apparatus. The system comprised a Nd:glass laser of adjustable power (wavelength 1054 nm, pulse width 0.3 ms) for flashing one side of the sample, and a liquid N_2-cooled MCT infrared detector for recording the increase of temperature on the opposite side. This method was used since it allows evaluating the thermal properties of small and thin samples, unlike usual methods of thermal conductivity measurement. Samples were cut into squares of dimensions 10 × 10 mm, and their thickness was cautiously measured with an electronic calliper. All samples presenting non-flat surfaces and/or inhomogeneous thickness were discarded. The films were then installed in a SiC sample holder, and submitted to laser pulses (3 pulses separated by 5min) of power around 5 mJ. The corresponding temperature increase was recorded, and the curve was fitted by the *Proteus*® software, using the radiation-corrected model. Because the method requires perfect thickness homogeneity, which is very hard to achieve with OLC/PU composite films, only a few selected samples could be accurately investigated.

Results and discussion

Room temperature dielectric properties and composite structure

TEM images of OLC particles used in the present study and having average aggregate sizes of 40 nm and 100 nm are presented in Fig. 1. The left part of Fig. 1 illustrates low-magnification TEM images of the aggregates while the right part presents their high-resolution images. One can see that the primary OLC particles consist of defective fullerene-like shells, combined into aggregates with joint graphene layers rather similar to what is known for some carbon blacks. Therefore, it is likely that OLC form chainlike clusters. Whereas the latter don't have any particular shape, they can probably deform easily when submitted to shear stress during the preparation of the composite: chains of carbon onions arranged in a pearl necklace structure are thus expected to be produced in the polymer matrix.

SEM images of OLC/PU composites with different aggregate sizes are presented in Fig. 2. It can be concluded that OLC particles are well dispersed in all cases, since all areas strictly looked equal, without obvious segregation or depletion at any place.

The frequency dependencies of dielectric permittivity and electrical conductivity for large aggregate size OLC/PU are presented in Fig. 3. The dielectric permittivity of composites with 3.5 vol. % of OLC inclusions and pure PU is very low (less than 10) and almost constant in a wide frequency range, while the electrical conductivity of these materials strongly increases with

frequency and no DC conductivity can be observed. Dielectric losses (which are strongly related with electrical conductivity) of these materials are also very low and caused by PU molecules dynamics [14]. Above an OLC concentration of 7 vol. %, the dielectric permittivity starts decreasing with frequency, whereas a constant conductivity can be observed at low frequency (DC conductivity), as well as two different dielectric dispersions obviously related to Maxwell-Wagner relaxation [23]. Therefore, the percolation threshold in composites with large OLC aggregates is close to 7.1 vol. % concentration, while similar considerations of composites with small OLC aggregates allowed determining the percolation threshold value close to 5.4 vol. %. Assuming that chains of carbon onions arranged in a pearl necklace structure are formed in the composite, as explained in the introduction, it is expected that aggregates based on small-sized OLC are more easily deformable, leading to more elongated aggregates in the polymer and hence to a lower percolation threshold. The present results agree with such assumption. The percolation threshold value close to 5.4 vol. % for small-sized OLC is slightly lower than the percolation threshold observed in OLC/polydimethylsiloxane composites for the same aggregate size [15]. The huge values of dielectric permittivity and electrical conductivity in the microwave range (for example at 30 GHz) of composites above the percolation threshold indicate that those composites are suitable for electromagnetic shielding. It can also be assumed that

The concentration dependence of both dielectric permittivity and electrical conductivity for different OLC aggregate sizes is presented in Fig. 4. The electrical conductivity values were selected at 129 Hz frequency, since above the percolation threshold those values correspond to the DC conductivity. According to the classical percolation theory, the filler concentration dependence of both dielectric permittivity ε' and electrical conductivity σ' above the percolation threshold follows power laws with different critical exponents g and t [24]:

$$\varepsilon' = \varepsilon_p (f - f_c)^g \quad (1)$$

$$\sigma' = \sigma_p (f - f_c)^t \quad (2)$$

where f and f_c are the volume fraction and the critical volume fraction (percolation threshold) of filler, respectively, and ε_p and σ_p are the permittivity and the conductivity of the filler, respectively. Obtained parameters are $\varepsilon_p = 62.3 \times 10^3$, $g = 1.26$, $\sigma_p = 320$ S/m, $t = 3.5$, $f_c = 0.054$ for 40 nm OLC aggregate size, and $\varepsilon_p = 228.7 \times 10^3$, $g = 1.25$, $\sigma_p = 2.4$, $t = 1.5$ for 100 nm OLC aggregate size.

Frequency dependencies of the electrical conductivity of composites with 7.1 vol. % of OLC at different temperatures are presented in Fig. 5. At low frequency, and as expected just above the percolation threshold, a frequency-independent plateau (DC conductivity) is observed but at higher frequency the conductivity increases as a power law of frequency. On cooling, the DC conductivity decreases and the changes of conductivity behaviour can be fitted by Almond-West power law:

$$\sigma(\omega) = \sigma_{DC} + K \omega^s \quad (3)$$

where σ_{DC} and $K \omega^s$ are DC and AC conductivity, respectively. From this fit, the critical frequency at which the conductivity starts to increase from its DC values (here an increase by 10% was chosen) can be calculated. The resultant parameters are presented in Fig. 6.

Below room temperature, the DC conductivity can be described by fluctuation-induced tunnelling model, as presented in Fig. 6:

$$\sigma_{DC} = \sigma_{DC0} \exp\left(-\frac{T_1}{T+T_0}\right) \quad (4)$$

where σ_{DC0} is the conductivity at very high temperatures ($T>>T_1$ and T_0), T is the absolute temperature, T_1 represents the energy required for an electron to cross the insulator gap between the conductive particles aggregates, and T_0 is the temperature above which thermally activated conduction over barriers starts to occur. The corresponding parameters are gathered in Table 1. According to the tunnelling model:

$$T_1 = \frac{w\,A\,\beta_0}{8\,\pi\,k} \tag{5}$$

$$T_0 = \frac{2\,T_1}{\pi\,\chi\,w} \tag{6}$$

where $\chi = (2\,mV_0)^{0.5}/\,h$ and $\beta_0 = 4V_0\,/\,ew$, m and e being the electron mass and charge, respectively, h is the Planck constant, V_0 is the potential barrier height, w is the inter-particle distance (gap width), and A is the area of the capacitor formed by the junction.

However, at even lower temperatures, typically below 100 K, Mott's law describes also quite well the temperature dependence of the electrical conductivity (Fig. 7). It reads:

$$\sigma_{DC} = \sigma_{DC0} \exp\left[-\left(\frac{T_m}{T}\right)^{1/n}\right] \tag{7}$$

where T_m is a constant depending on the density of states and localisation length of the system, and $n = 1 + d$, d being the dimensionality of the system. The resultant parameters are given in Table 2, where it can be seen that the values of σ_{DC0} derived from the fits of either Eq. (4) or Eq. (7) to the experimental data are quite consistent with each other. The dimensionality for all composites is close to 0.5, which is typical for pure OLC obtained by annealing nano-diamonds at 1600 K [7]. Below 100 K, the critical frequency decreases on cooling according to the law:

$$f_{cr} = f_\infty \exp\left[-\left(\frac{T_m}{T}\right)^{1/n}\right], \tag{8}$$

where f_∞ is the frequency at very high temperature. For one-dimensional hopping conductivity, the dc hopping length reads:

$$R_{dc} = \sqrt{\frac{\Delta r}{2\,\alpha\,T}} \tag{9}$$

while the ac hopping length is:

$$R_{ac} = \frac{1}{2}\alpha \ln\frac{f_{fon}}{f_{cr}} \tag{10}$$

where Δ determines an uniform distribution of carriers energies, r is the distance between two nearest OLC particles, α^{-1} is the localisation length, and f_{fon} is the attempt frequency. Assuming that both localisation length and attempt frequency don't depend on temperature and concentration, it can be concluded that the increase of critical frequency f_{cr} with OLC concentration seen in Fig. 7(b) is related to the decrease of ac hopping length, while the increase of critical frequency with temperature is related to the decrease of ac hopping length. Thus, the electrical transport in PU matrices filled with OLC of different aggregate sizes proceeds by electron hopping inside OLC clusters and by tunnelling between clusters.

The results of thermal diffusivity measurements are presented in Fig. 8. The thermal diffusivity, being the quantity describing the ability of the materials to rapidly transmit the heat, increases with OLC concentration. Since thermal conductivity is the product of diffusivity × heat capacity × bulk

density of the material, and since heat capacity and density can be easily calculated by rules of mixtures, it is expected that the thermal conductivity presents the same qualitative behaviour as the diffusivity. As for the effect of OLC aggregate size, the thermal diffusivity is higher for composites with smaller filler, in agreement with their higher electrical conductivity although the effect is far lower here, since no percolation occurs.

Conclusion

Composite films based on polyurethane (PU) matrix filled with various volume fractions of onion-like carbon (OLC) having two aggregate sizes, 40 and 100 nm, were investigated by dielectric/electrical and thermal diffusivity studies. The lowest percolation threshold in such materials was determined as 5.4 vol. % in the case of 40 nm OLC aggregate size. The huge values of dielectric permittivity and electrical conductivity in the microwave range (for example at 30 GHz) of composites above the percolation threshold indicate that those composites are suitable for electromagnetic shielding. The electrical transport in OLC/PU composite films is controlled by quasi-one-dimensional electron hopping inside OLC clusters on the one hand, and by tunnelling between OLC clusters on the other hand. The thermal diffusivity increases with OLC concentration, as expected, and is higher for composites with smaller OLC aggregates, in agreement with the lower percolation threshold evidenced by electrical conductivity measurements.

Acknowledgements The authors gratefully acknowledge the financial support of “Gilibert” PHC exchange project “Dielectric and electric properties of hollow carbon spheres and mesoporous carbon between Lithuania and France”. The French team gratefully acknowledges the financial support of the CPER 2007–2013 “Structuration du Pôle de Compétitivité Fibres Grand'Est” (Competitiveness Fibre Cluster, France), through local (Conseil Général des Vosges), regional (Région Lorraine), national (DRRT and FNADT) and European (FEDER, France) funds.

References

[1] F. Qin and C. Brosseau, J. Appl. Phys. **111**, 061301 (2012).

[2] Z. Han, A. Fina, Progress in Polymer Science **36**, 914 (2011).

[3] S. Kirkpatrick, Rev. of Modern Physics **45**, 574 (1973).

[4] W. Bauhofer, Z. Kovacs, Composite Science and Technology **69**, 1486 (2009).

[5] L. J. Adriaanse, J. A. Reedijk, P. A. A. Teunissen, H. B. Brom, M. A. J. Michels and J. C. M. Brokken-Zijp, Phys. Rev. Lett. **78**, 1755 (1997).

[6] K. Kostarelos, Nature Biotechnology **26**, 774 (2008).

[7] V. L. Kuznetsov, Yu. V. Butenko, A. L. Chuvilin, A. I. Romanenko, A. V. Okotrub, Chemical Physics Letters **336**, 397 (2001).

[8] S. Kang, J. E. Kim, D. Kim, C. G. Woo, P. V. Pikhitsa, M. H. Cho, M. Choi, Journal of nanoparticle research 17, 378 (2015).

[9] J. Batelmess, S. Giordani, Belstein journal of Nanotechnology 5, 1980 (2014).

[8] S. A. Maksimenko, V. N. Rodionova, G. Y. Slepyan, V. A. Karpovich, O. Shenderova, J. Walsh, V. L. Kuznetsov, I. N. Mazov, S. I. Moseenkov, A. V. Okotrub, P. Lambin, Diamond and related materials 16, 1231 (2007).

[9] J. Macutkevic, P. Kuzhir, D. Seliuta, G. Valusis, J. Banys, A. Paddubskaya, D. Bychanok, G. Slepyan, S. Maksimenko, V. Kuznetsov, S. Moseenkov, O. Shenderova, A. Mayer, Ph. Lambin, Diamond & related materials **19**, pp. 91-99 (2010).

[10] R. Langlet, P. Lambin, A. Mayer, P. P. Kuzhir, S. A. Maksimenko, Nanotechnology **19**, 115706 (2008).

[11] J. Macutkevic, R. Adomavicius, A. Krotkus, D. Seliuta, G. Valusis, S. Maksimenko, P. Kuzhir, K. Batrakov, V. Kusnetsov, S. Moseenkov, O. Shenderova, A. V. Okotrub, R. Langelet, Ph. Lambin, Diamond & related materials **17**, pp. 1608-1612 (2008).

[11] J. Macutkevic, D. Seliuta, G. Valusis, J. Banys, V. Kuznetsov, S. Moseenkov, O. Shenderova, App. Phys. Lett. **95**, 112901 (2009).

[12] S. Kirkpatrick, Phys. Rev. Lett. **36**, 69 (1976).

[13] Y. Y. J. Deng and H. W. J. Blote, Phys. Rev. E **72**, 013126 (2005).

[14] P.P Kuzhir, A. G. Paddubskaya, S. A. Maksimenko, V. L. Kuznetsov, S. Moseenkov, A. I. Romanenko, O. A. Shenderova, J. Macutkevic, G. Valusis, P. Lambin, IEEE Transactions on Electromagnetic Compatibility **54**, 6 (2012).

[14] J. Liang and Q. Yang, J. Appl. Phys. **102**, 083508 (2007).

[15] J. Macutkevic, I. Kranauskaite, J. Banys, S. Moseenkov, V. Kuznetsov, O. Shenderova, Journal of Applied Physics **115**, 213702 (2014).

[16] J. Macutkevic, R. Adomavicius, A. Krotkus, J. Banys, V. Kuznetsov, S. Moseenkov, A. Romanenko, O. Shenderova, Journal of Applied Physics 111**,** 103701 (2012).

[17] J. Grigas, *Microwave dielectric spectroscopy of ferroelectrics and related materials*, Gordon and Breach Science Publ., OPA Amsterdam (1996).

[18] K. Bertulis, A. Krotkus, G. Aleksejenko, V. Pacebutas, R. Adomavicius, G. Molis, S. Marcinkevicius, Appl. Phys. Lett. **88**, 201112 (2006).

[19] I. Pupeza, R. Wilk, M. Koch, Optics Express **15**, 4335 (2007).

[20] S. R. Tripathi, M. Aoki, M. Takeda, T. Asahi, I. Hosako, N. Hiromoto, Jap. J. Appl. Phys. **52**, 042401 (2013).

[21] J. Liu, Ch. G. Duan, W. G. Yin, W. N. Mei, R. W. Smith and J. R. Hardy, Phys. Rev. B **70**, 144106 (2004).

[22] D. J. Bergman, Phys. Rev. Lett. **44**, 1285 (1980).

Tables

Table 1. Tunnelling fit parameters for DC conductivity at low temperatures.

OLC aggregate size	Concentration, vol.%	σ_{DC0}, mS/m	T_1, K	T_0, K
Large	7.2	0.93	53	11
	9.5	16.9	36	7
	11	27	39	8
	12	10.5	31	7
	14	250	36	8
Small	5.4	0.006	63	3
	7.3	0.285	54	9
	8.4	8.18	58	6
	9.2	1.6	62	15
	11	22.7	53	7

Table 2. Mott's law fit parameters for DC conductivity at low temperatures

OLC aggregate size	Concentration, vol.%	σ_{DC0}, mS/m	T_m, K	n	ω_0, kHz
Large	7.2	1.12	55	1.51	14.472
	9.5	17	31	1.24	268.874
	11	35.7	45	1.73	2213.310
	12	99	29	1.41	481.663
	14	254	29	1.09	-
Small	5.4	25.73	78	1.35	21.162
	7.3	0.33	56	1.46	81.226
	8.4	9.28	54	1.12	830.680
	9.2	2	64	1.62	402.834
	11	25.73	54	1.37	-

Figures

Fig. 1 TEM images of OLC with 40 nm and 100 nm average aggregate size. Left part—low magnification images of aggregates deposited on the amorphous carbon layer of TEM grid. Right part presents of HR TEM images of OLC aggregates.

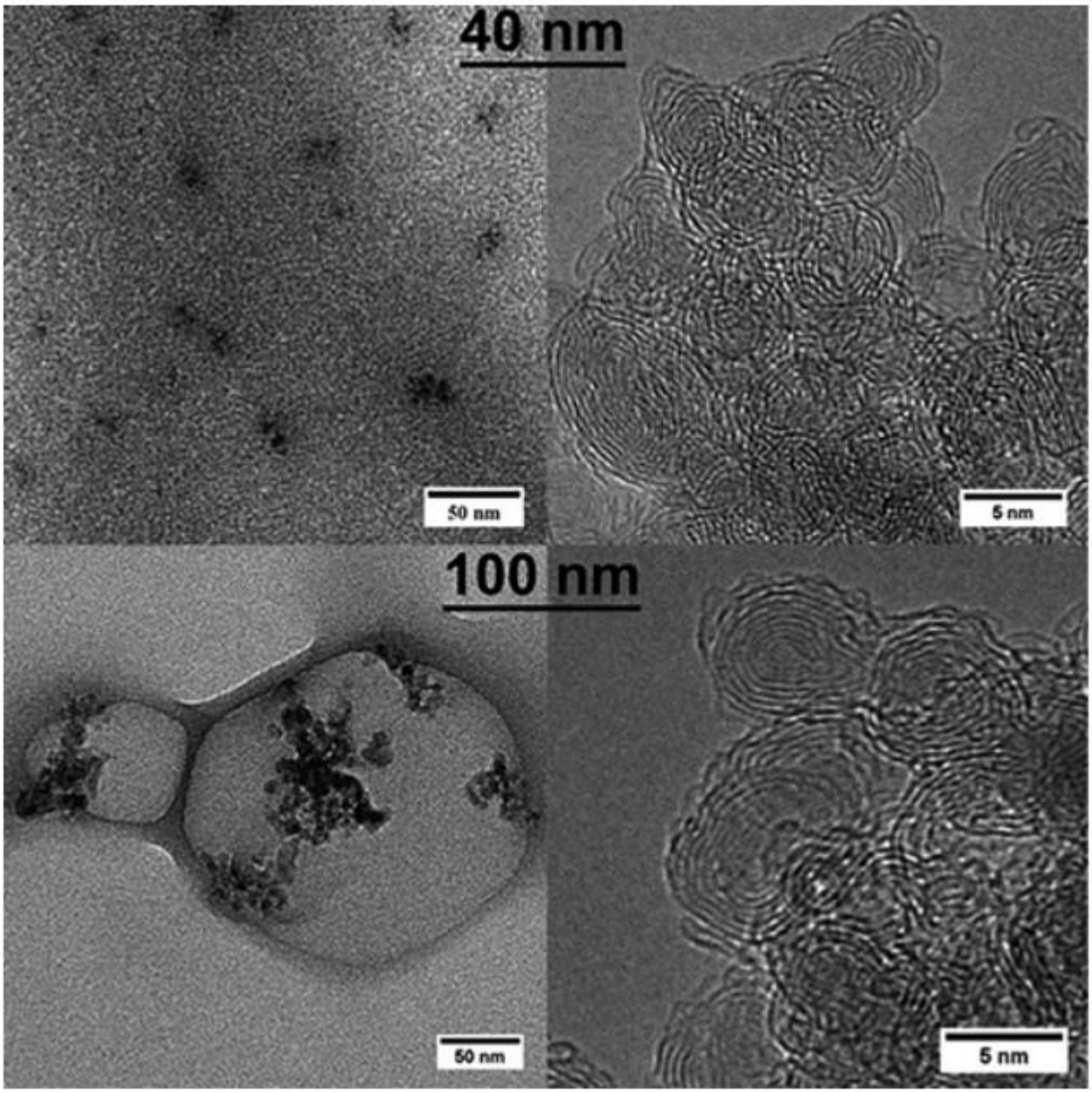

Fig. 2. SEM images of composite films based on polyurethane matrix filled with: (a) 14 vol. % of OLC of aggregate size 100 nm, (b) 11 vol. % of OLC of aggregate size 40 nm; (c) 3.5 vol. % of OLC of aggregate size 100 nm.

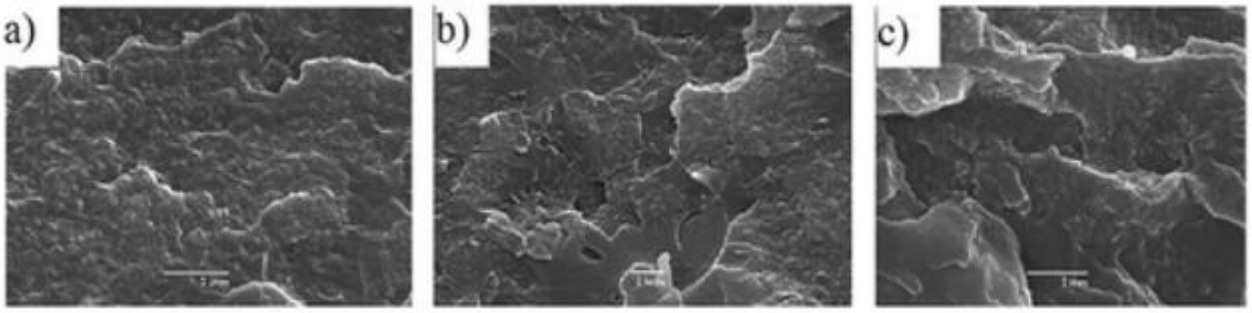

Fig. 3. Frequency spectra of real parts of complex dielectric permittivity and electrical conductivity of OLC/PU composites (with large OLC inclusions) at room temperature.

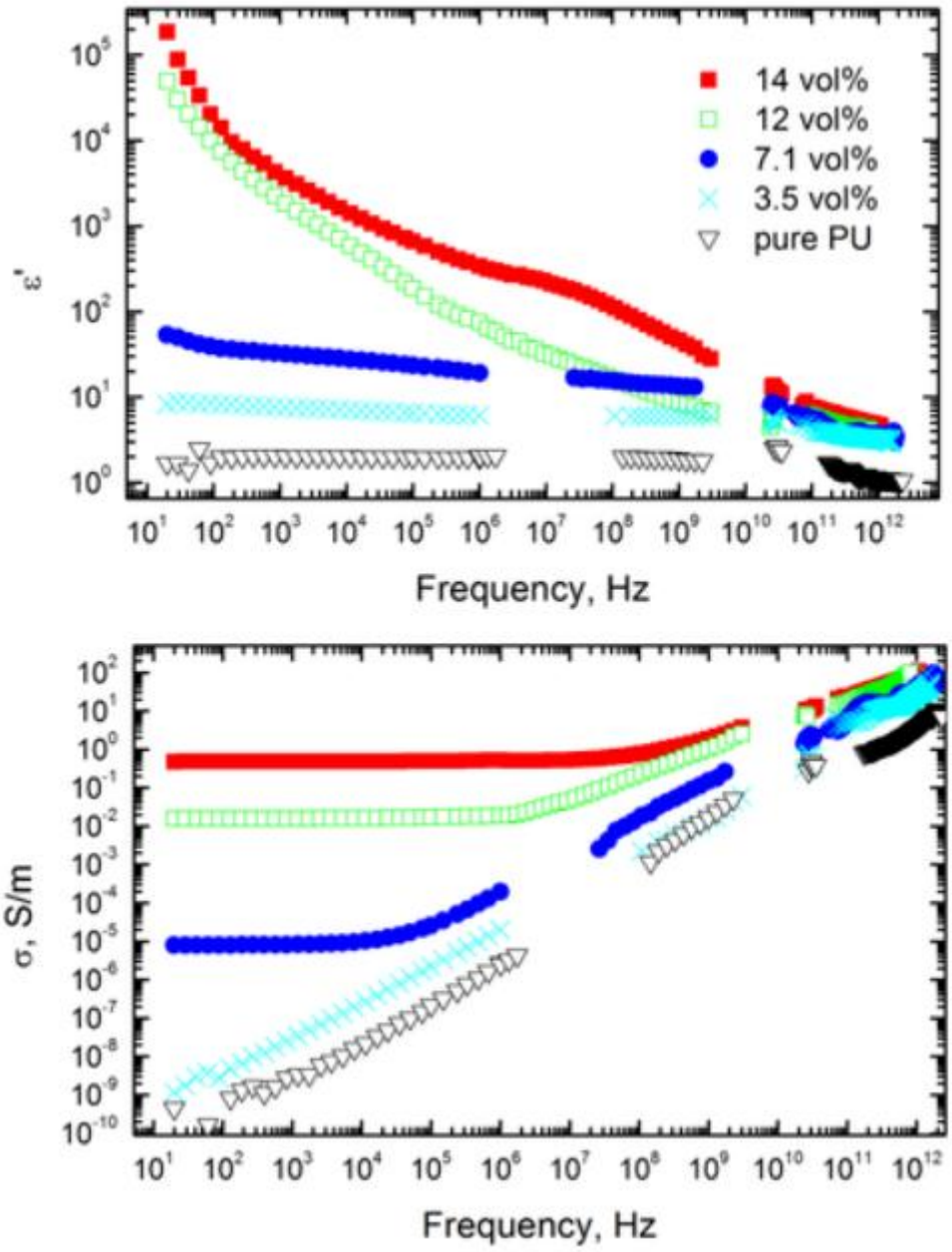

Fig. 4. Real parts of complex dielectric permittivity and complex electrical conductivity of OLC/PU composites vs. OLC concentration and aggregate size at frequency 129 Hz and room temperature.

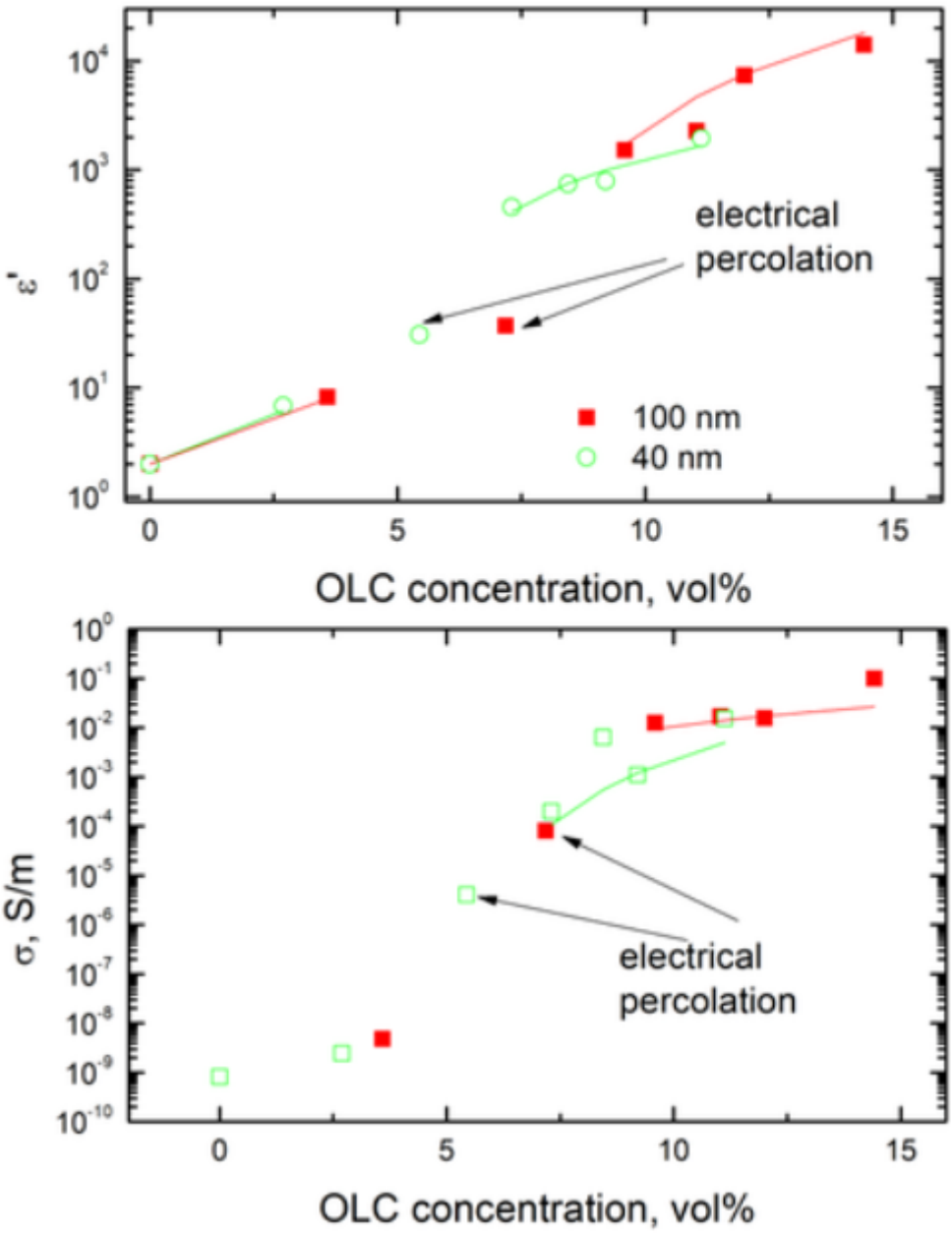

Fig. 5. Frequency dependence of the real part of complex electrical conductivity of OLC/PU (with 100 nm OLC inclusions at 7.5 vol. %) at different temperatures (low-temperature region).

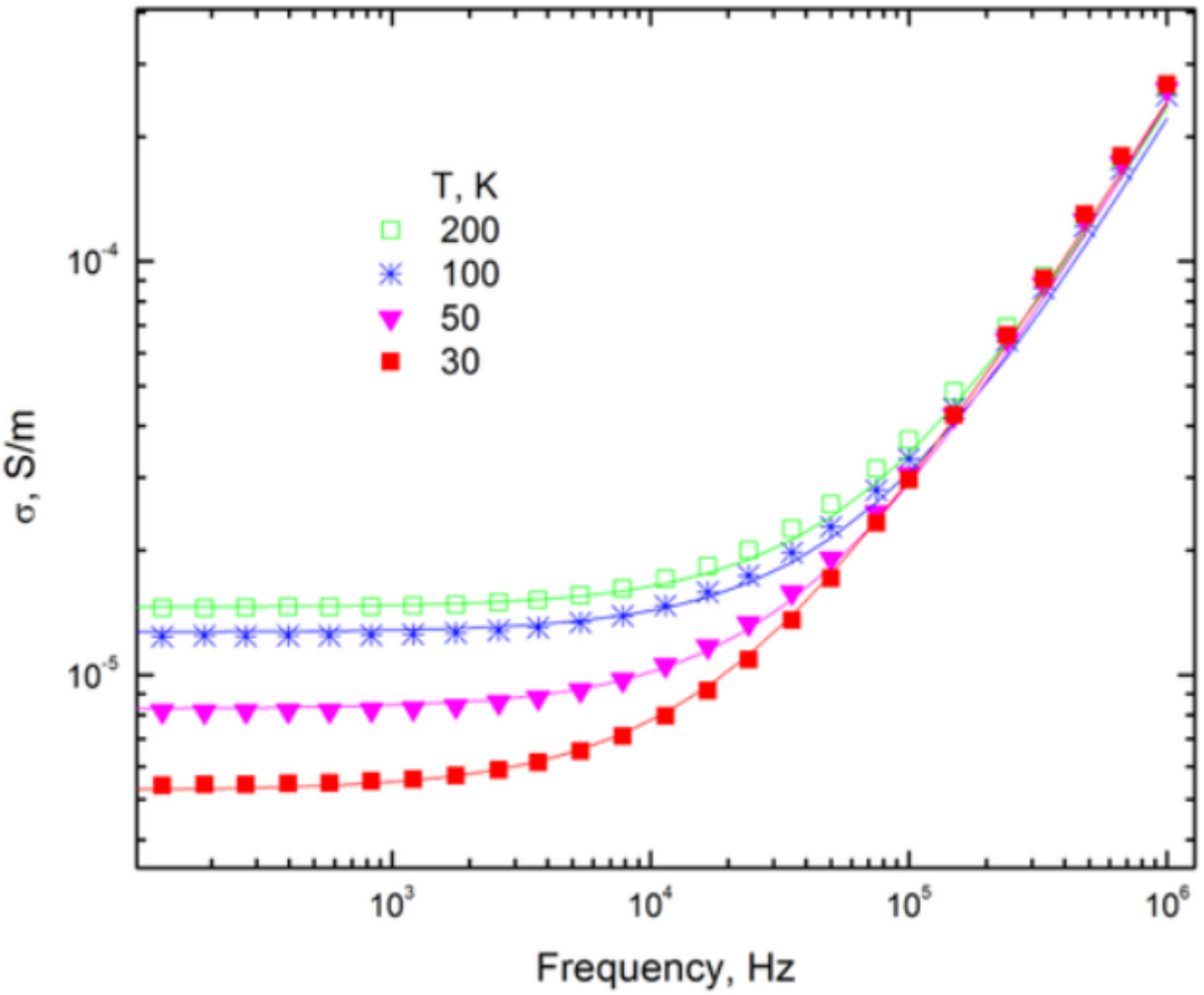

Fig. 6. Temperature dependence of OLC/PU composites DC conductivity fitted by tunnelling law (Eq. (4)) in the low-temperature region.

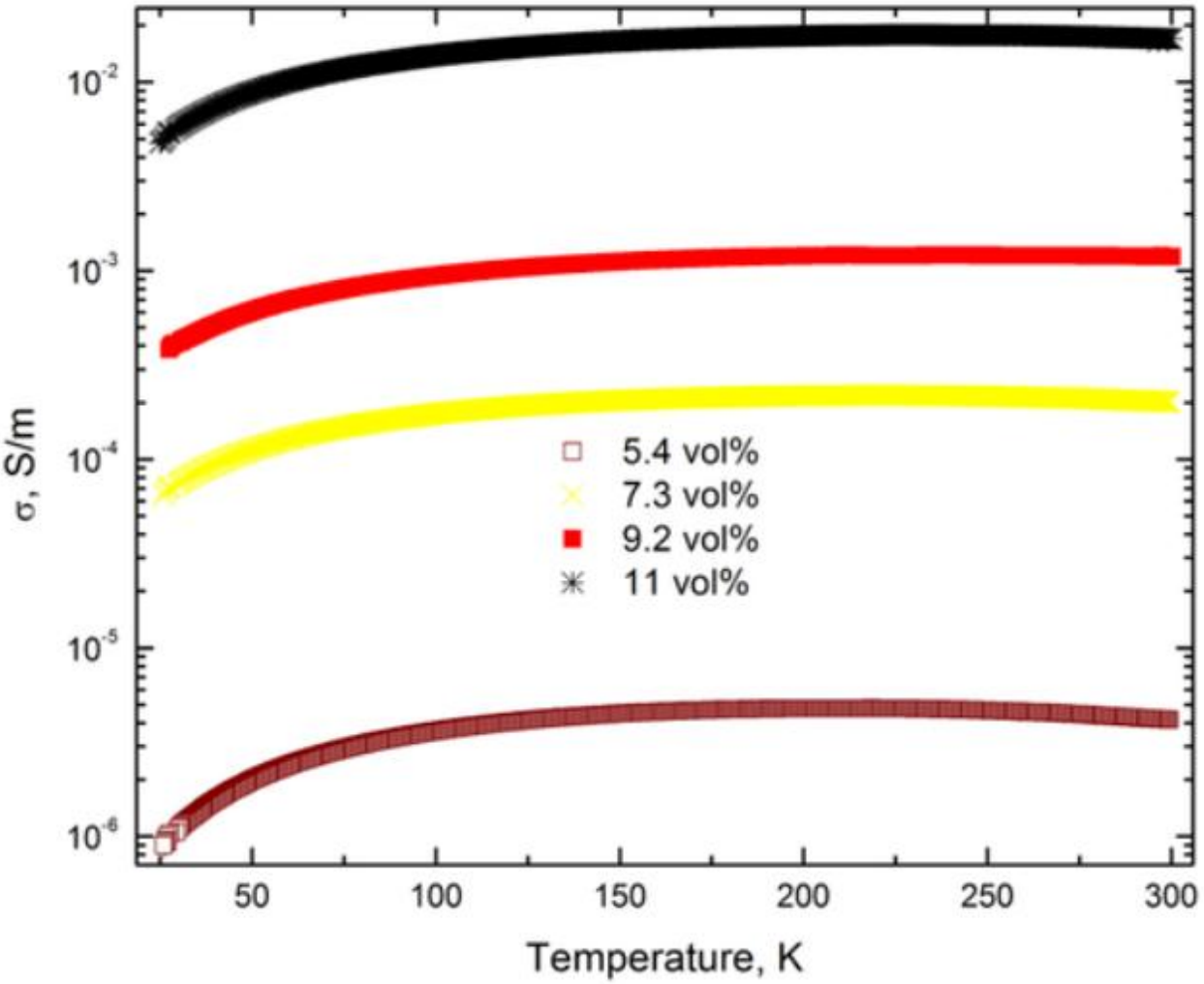

Fig. 7. (a) Temperature dependence of OLC/PU composites DC conductivity fitted by Mott's law (Eq. (7)) in the low-temperature region; and (b) corresponding critical frequency.

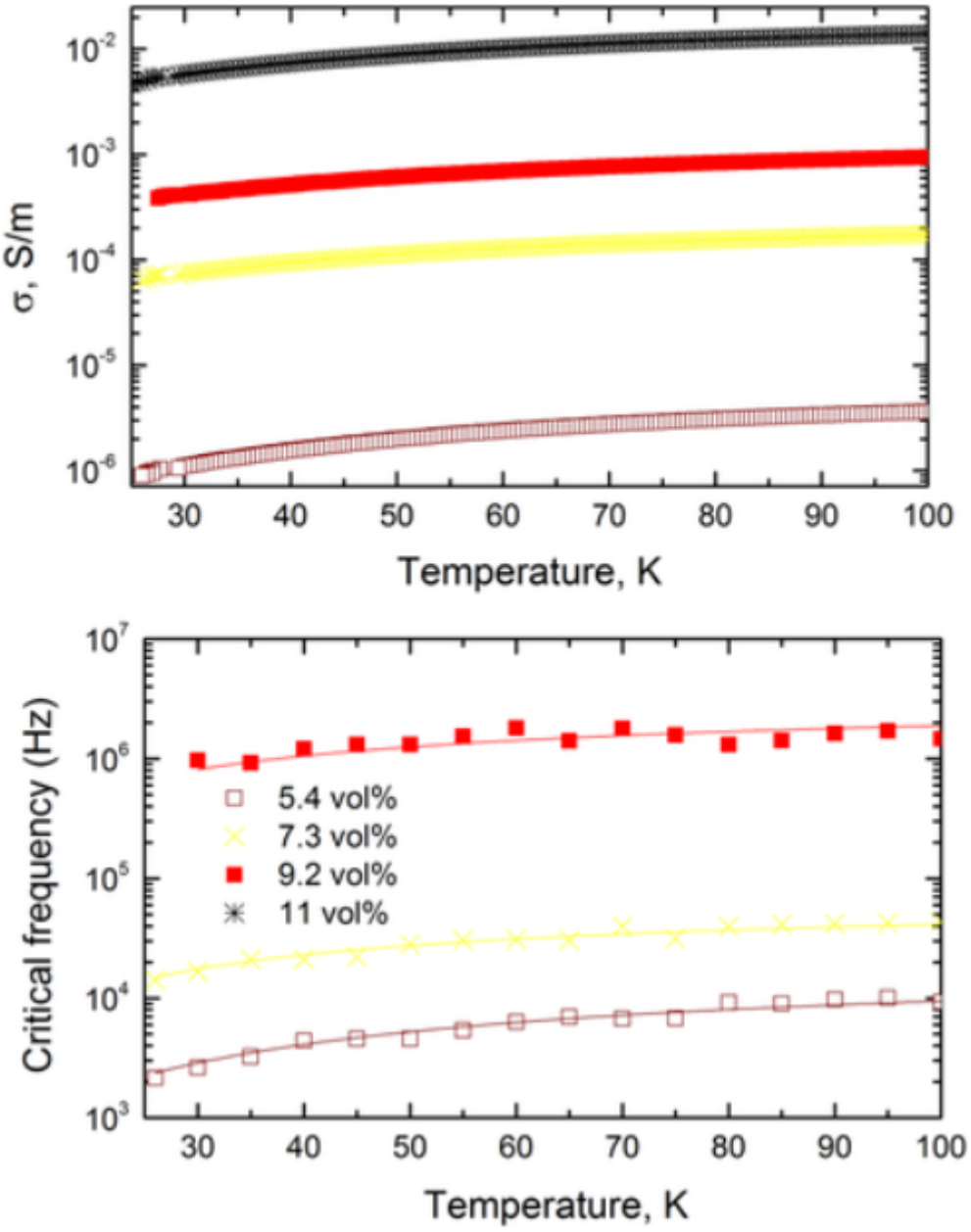

Fig. 8. Thermal diffusivity of OLC/PU composites as a function of OLC concentration and aggregate size.